machines

MDPI

Article

Evaluation of Load-Bearing Performance and Cost Efficiency in Steel-Welded and Modular Aluminum Rack Structures

Lenka Jakubovičová [1], Milan Vaško [1] and František Synák [2,*]

[1] Department of Applied Mechanics, Faculty of Mechanical Engineering, University of Zilina, 010 26 Žilina, Slovakia; lenka.jakubovicova@uniza.sk (L.J.); milan.vasko@fstroj.uniza.sk (M.V.)
[2] Department of Road and Urban Transport, Faculty of Operation and Economics of Transport and Communications, University of Zilina, 010 26 Žilina, Slovakia
* Correspondence: frantisek.synak@uniza.sk; Tel.: +421-41-513-3505

Abstract: The profile modular system offers variability, flexibility, ease of assembly, and corrosion resistance as well as non-time-consuming assembly while meeting the required conditions of the customer. It has a broad spectrum of usability. This article compares the results of a stress analysis solution for two variants of a rack structure, namely the original variant made by welding Jäkl profiles and the newly proposed design variant created with aluminum Bosch profiles. The finite element method (FEM) is used in computational analyses. FEM models are created using shell elements. Particular attention is given to the use of shell elements in the FEM and their suitability for finite element analyses of the selected structures. Finally, the advantages and disadvantages of both approaches are evaluated, including a safety assessment and an economic comparison of the variants.

Keywords: FEM analysis; buckling analysis; shell element; frame structure; eigenvalue buckling analysis

check for updates

Academic Editor: Raul D. S. G. Campilho

Received: 15 April 2025
Revised: 29 May 2025
Accepted: 3 June 2025
Published: 10 June 2025

Citation: Jakubovičová, L.; Vaško, M.; Synák, F. Evaluation of Load-Bearing Performance and Cost Efficiency in Steel-Welded and Modular Aluminum Rack Structures. *Machines* **2025**, *13*, 506. https://doi.org/10.3390/machines13060506

Copyright: © 2025 by the authors. Licensee MDPI, Basel, Switzerland. This article is an open access article distributed under the terms and conditions of the Creative Commons Attribution (CC BY) license (https://creativecommons.org/licenses/by/4.0/).

1. Introduction

Racks, in general, form an integral part of production lines, storage spaces, and storage areas in households [1–3]. In the production process and industrial settings, racks must meet the specific required load-bearing capacity and the storage capacity for materials and components [4–6]. From a design perspective, they must also comply with workplace safety conditions to ensure they do not pose a threat to the operating personnel [7–9]. Therefore, it is essential to perform a strength analysis for these constructions [10,11]. The study [12] presents an analysis of 16 aluminum cross-section profiles using finite element analysis (FEA) in ABAQUS, especially for stocky or slender cross-sections. Under the specified loading conditions, a stability loss analysis is necessary to prevent the structure from collapsing, which could result in damage to stored components and, in the worst case, pose a risk to human health [13,14]. When racking systems are in areas with specific conditions, more attention is paid to the analyses themselves than in the study by [15], where a realistic assessment of the effectiveness of a roller-base isolation system in reducing seismic responses and improving the stability of industrial steel storage racks was analyzed [15]. In situations involving the induced loss of stability, this also creates a hazardous condition for both equipment and personnel [16,17]. To verify this risk, it is crucial to perform an Eigenvalue Buckling analysis of the loaded frame structure [18–20]. The research [21] identifies distinct failure mechanisms that are dependent on slenderness—local buckling for short columns, combined distortional–flexural buckling for medium-length columns, and global flexural

buckling for slender columns. The use of the rack structure is versatile. The modular rack-based construction in Noonan et al.'s study supports scalability, consistent illumination, and compatibility with standard microplate formats, thereby enhancing the efficiency of photosynthetic microorganism screening [22]. The rack-based construction in Yu et al.'s study was implemented to enable the synchronous grafting of six vegetable seedlings, and the design facilitates the precise alignment and coordination of key components, ensuring consistent grafting quality across multiple seedlings simultaneously [23]. An experimental study of the behavior of stiffened, perforated cold-formed steel (CFS) uprights commonly used in industrial storage racks can be found in the study [24].

Most research examines either welded or modular constructions in isolation [9]. The study [25] presents five structural framing methods for building information model (BIM)-based prefabricated MEP racks, demonstrating through pilot testing that optimizing frame components and support spacing can significantly reduce material and labor costs. The article [26] provides a comparative analysis of conventional steel frame warehouses and rack-supported warehouse structures, focusing on aspects such as construction processes, storage capacity, economic viability, and flexibility of usage. The article [27] by Mela and Heinisuo presents a method for optimizing the weight and cost of welded high-strength steel beams, demonstrating that significant material savings and economic benefits can be achieved through advanced structural optimization techniques.

Our work stands out by directly comparing these two approaches, offering insight into their respective advantages and trade-offs. In addition to comparing the two methods, the novelty of this article lies in the addition of an economic analysis. Comparing these two approaches and comparing them from an economic perspective thus allows for a truly comprehensive comparison of both methods, which is the main novelty of this article. Based on the literature review, it can be concluded that the comparison of two strength analysis methods is uncommon and offers the advantage of consolidated information within a single article [28–30]. At the same time, this work contributes to the relatively underrepresented scientific literature on rack dimensioning, despite the fact that racks constitute a crucial part of logistics [31,32]. The selection of specific beams and their subsequent analysis enhances the importance of this article for the professional public, as the knowledge presented in this publication can be used for specific cases from practice [33].

2. Methodology and Results

The following text contains the methodology for performing finite element analyses of both the original welded structure and the newly assembled structure, along with the corresponding results. For both constructions, a model was first created, followed by the definition of boundary conditions and the evaluation of critical points. The economic assessment of both variants is presented at the end of the section.

2.1. Assignment Presentation

The requirement of the practice was to design a new racking system that meets the conditions of flexibility, corrosion resistance, and variability. The welded structure constructed from Jäkl profiles is a commercially implemented solution developed for a specific customer, with permission granted for its use in this study. The authors analyzed two different variants of the frame structure. The newly designed variant of the racking system consists of Bosch Rexroth aluminum profiles. The original functional frame structure, installed on the production line, is made of welded Jäkl-type steel profiles. Both variants of the solution will be compared at the end in terms of production costs, material and labor expenses, and the time required for the design and manufacturing process.

The welded structure placed in an automated welding line (Figure 1) was designed and manufactured based on engineers' experience, with significant over-dimensioning [34,35]. No attention was given to strength analysis. The construction, made from Jäkl profiles and the fact that it is fully welded, makes it a solid, unchanging, and robust storage rack. Over time, a request for a change in access from the rear side arose, which led to the need to create a variable structure while meeting all strength and safety conditions and while maintaining the functional requirements [35–38].

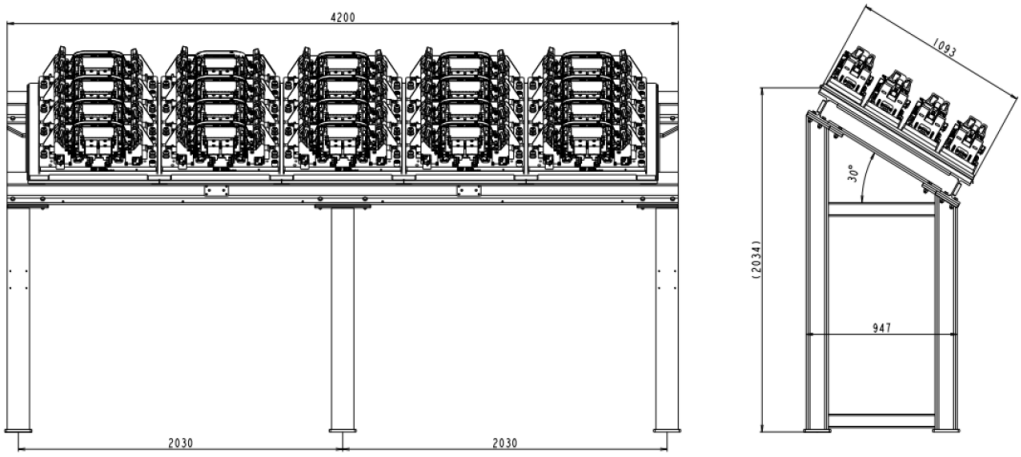


Figure 1. The drawing of the rack with its basic dimensions.

In the first step, the existing welded steel structure was analyzed (Figure 1). It is primarily a welded construction, consisting mainly of I-shaped profiles with dimensions of 100 × 100 mm. The crossbars on the vertical supports have a rectangular cross-section (Jäkl profiles) with dimensions of 80 × 80 mm. The individual parts of the welded subassemblies are connected using bolted joints.

The rack (4) is positioned between two automated welding towers (1), where parallel friction welding, also known simply as friction welding, takes place. A detailed view of the entire workstation, including the placement of the rack, is shown in Figure 2.

The loading and unloading of welding fixtures from the rack (4) to the welding tower (1) (from the welding tower (1) to the rack (4)) will be carried out automatically using an ABB IRB 6700 industrial robot (2). The production line is designed for manufacturing various semi-finished product variants. These semi-finished products differ primarily in the relative positioning of the workpieces during the welding process, which is ensured by the use of welding fixtures. Each fixture has an average weight of 100 kg, and the rack has the capacity to store up to twenty fixtures. Two vibratory feeders (3) are located beneath the rack, which are accessible to the human operator. Therefore, the personnel can be located beneath the rack structure during the unloading of the fixture by the robot, and thus in the area where the robot has reach. It is crucial to ensure that the structure is sufficiently rigid, as any failure could pose a risk to the operating personnel.

The required flexibility and variability of the new beam structure will be achieved using aluminum profiles from Bosch Rexroth (Figure 3a). Emphasis is also placed on ensuring the necessary load-bearing capacity while maintaining safety in terms of structural strength and resistance to collapse due to stability loss. Additionally, in the case of induced oscillations, an analysis will be conducted to ensure that the structure does not enter its resonant frequency and subsequently lose stability. The original welded structure made of Jäkl profiles is shown in Figure 3b.

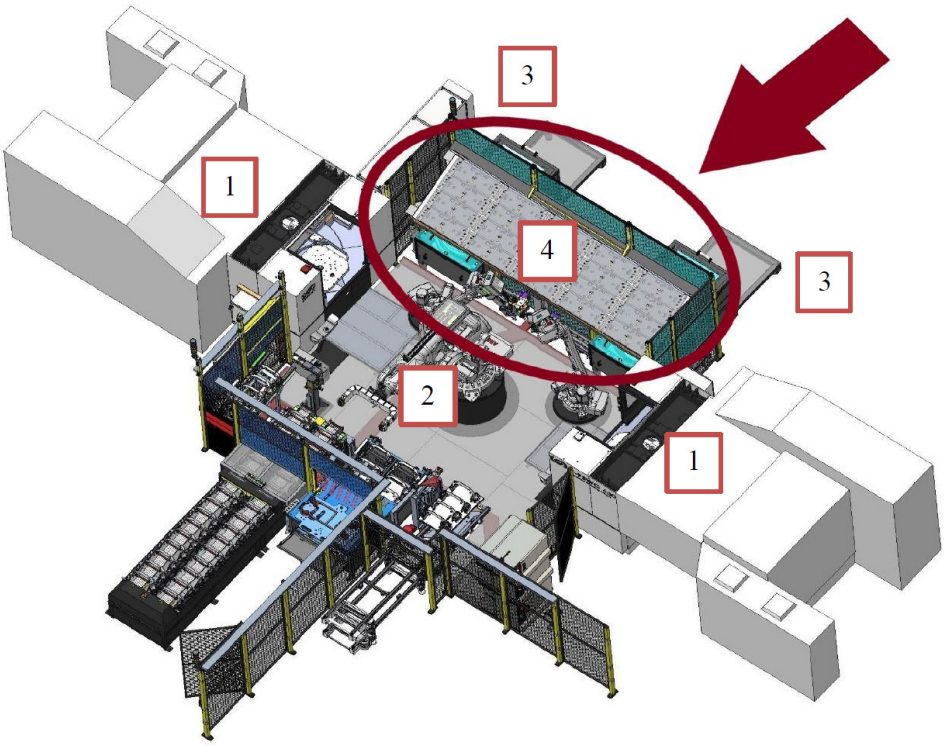
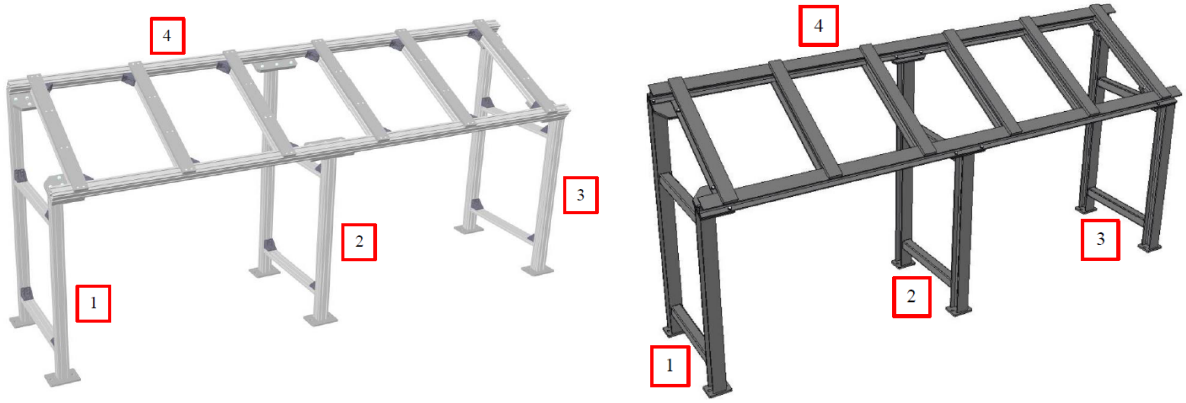


Figure 2. Automated welding line with the highlighted rack: (**1**) welding tower, (**2**) industrial robot, (**3**) vibratory feeder, (**4**) rack—in circle.



(**a**) (**b**)

Figure 3. Two variants of the supporting rack construction for welded components: (**a**) alternative rack construction made of Bosch Rexroth aluminum profiles labeled with individual assembled subassemblies; (**b**) rack construction for welding fixtures labeled with individual welded subassemblies. (**1**) Left upright, (**2**) middle upright, (**3**) right upright, (**4**) storage area.

2.2. Dimensioning and Strength Material Analysis

In more complex cases of planar and, especially, three-dimensional stress, the issue of finding a material's critical condition becomes more complicated, as its failure can occur under various combinations of principal stresses σ_1, σ_2, σ_3, and, therefore, it is not determined by just one numerical parameter. For the stress corresponding to the limit state, the strength condition for the allowable stress σ_D is given by Equation (1):

$$\sigma_D = \frac{R_e}{k}, \tag{1}$$

where R_e is the yield limit and k is the safety coefficient relative to the yield limit R_e.

Based on these criteria, we can determine a representative stress σ_{RED}, which can be compared with the results of the tensile test. Experimental measurements have shown that the hypothesis based on deformation energy for shape change, HMH (Hubert–Mises–Hencky), provides more accurate results than other well-known hypotheses [39]. The evaluation of results is performed using this hypothesis, Equation (2).

$$\sigma_{RED} = \frac{\sqrt{2}}{2} \cdot \sqrt{(\sigma_1 - \sigma_2)^2 + (\sigma_1 - \sigma_3)^2 + (\sigma_2 - \sigma_3)^2} < \sigma_D, \quad (2)$$

where

σ_{RED}—reduced stress;
σ_D—allowable stress;
$\sigma_1, \sigma_2, \sigma_3$—principal stress components.

Comparing the analytical solution (Figure 4) with two finite element models allows us to observe the advantages and disadvantages of the chosen solutions. The first model is created using beam elements, and the second uses shell elements.

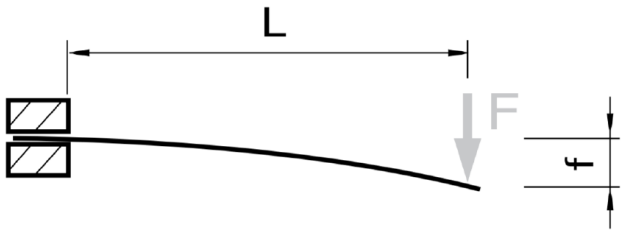


Figure 4. Schematic representation of a Bosch profile example (www.boschrexroth.com accessed on 20 March 2025).

Consider a simple example of a beam with a length of L = 1000 mm, fixed at one end and loaded with a force F = 500 N at the other end. The beam profile is a Bosch profile with dimensions 80 × 80 mm. The maximum deflection of the profile, f, is calculated as follows:

$$f = \frac{F \cdot L^3}{3 \cdot E \cdot I \cdot 10^4} = \frac{500\ \text{N} \cdot 1000^3\ \text{mm}^3}{3 \cdot 70{,}000 \cdot 132.1 \cdot 10^4} = 1.802\ \text{mm}. \quad (3)$$

where

F—applied force;
L—length of the beam;
E—modulus of elasticity in tension (Young's modulus);
I—moment of inertia of the beam's cross-section.

The material characteristics are taken from Table 1. For a comparison of the results, the value of the maximum bending stress, σ_{max}, is important, which we determine from the relation in the analytical solution, Equation (5):

$$\sigma_{max} = \frac{F \cdot L}{W_o \cdot 10^3} = \frac{500 \cdot 1000}{33 \cdot 10^3} = 15.151\ \text{MPa}. \quad (4)$$

The maximum bending stress in the Bosch profile 80 × 80 mm, loaded as shown in Figure 5, will be 15.151 MPa based on the analytical calculation. This value will be compared with the results obtained from the following two methods used for the finite element analysis performed in Ansys. Figure 5 shows a comparison of the stress analysis of the shell and solid elements. Table 1 shows the results for one selected profile to validate the modeling approach using shell elements.

Table 1. Percentage deviations of the maximum values of stress and displacement between the numerical and analytical solutions.

Calculation Variant	Maximum Displacement Value [mm]/Deviation	Maximum Stress Value [MPa]/Deviation
Analytical	1.802	15.151
Numerical (shell model)	1.687/6.38%	15.552/2.65%
Numerical (beam model)	1.851/2.72%	15.138/0.09%

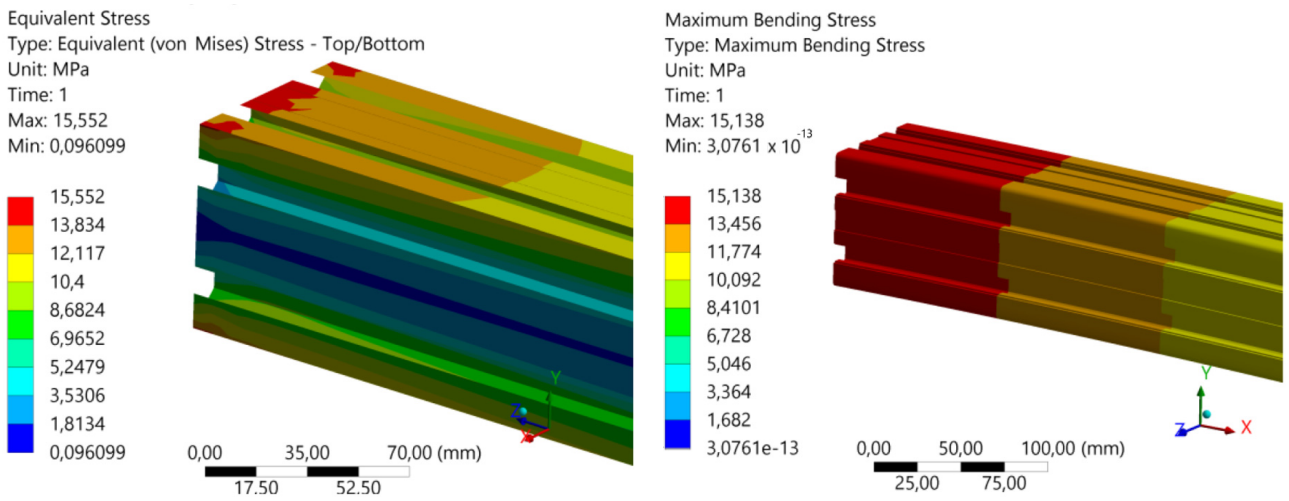


Figure 5. Bosch profile 80 × 80 mm, finite element results: (**a**) shell elements, (**b**) beam elements.

The element size was 7.5 mm for the shell model and 10 mm for the beam model. The highest stresses occur at the point of attachment of the Bosch profile, where the maximum bending moment is present. The maximum values of stress and displacement from both strength calculations and the theoretical calculation are summarized in Table 1.

The degree of agreement in both numerical solutions is sufficient, with the beam model providing more accurate results, as previously mentioned. Beam elements do not provide true stiffness in real body connections. In the case of beam elements, it is not possible to consider the screw preload. For this reason, the authors of the article decided to use shell elements in the modeling process.

3. Assembled Rack Structure

3.1. Design of an Alternative Structure Made of Aluminum Bosch Profiles

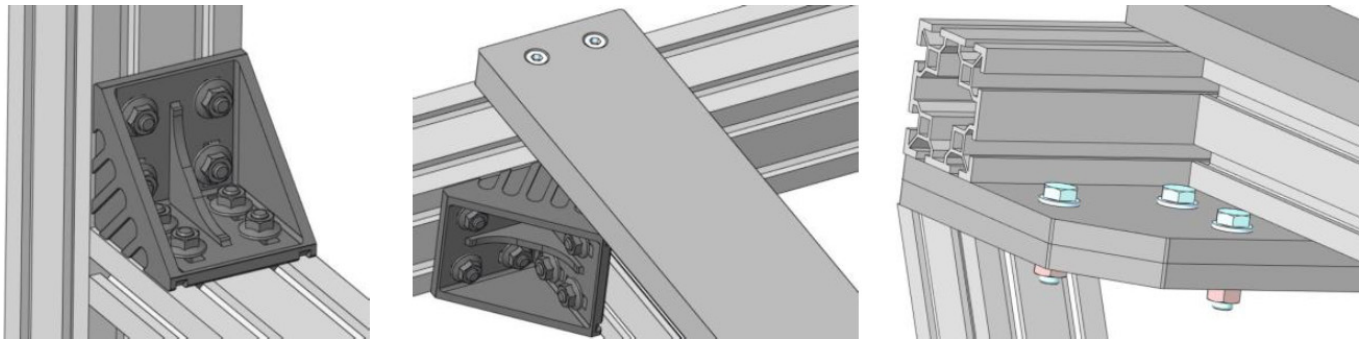
The use of Bosch profiles offers numerous advantages. The most fundamental advantage is the flexibility and variability they provide. This is associated with the possibility of reconfiguring according to the current requirements of the workplace and the potential for the repeated use of aluminum profiles. The entire system of fasteners, quick-release connectors, angles (Figure 5a,b), bolts, and universal joints up to 180° with 15° increments is used during the assembly process. A significant benefit is the quick assembly with a small number of assembly tools. The aluminum profile has high resistance to corrosion, reducing the need for regular surface maintenance [40,41]. Modular systems made from these profiles are increasingly preferred in the automotive industry [42].

The shape of the aluminum profiles is optimized and specifically designed to carry the maximum load with the minimum weight [43]. The T-shaped grooves serve a special

function when connecting Bosch profiles with other components of the structure. They contain threads, so there is no need to drill holes and weaken the profile.

3.2. Structural Model Made of Aluminum Profiles

At the beginning of every manufacturing process is the structural design, which provides the customer with insight into and vision of the future real construction. The 3D model of the assembled aluminum rack was created in the PTC Creo software, version 10.0.4.0 (Figure 3a). The design adhered to all external dimensions for placement in the welding line so that it could perform the same function as the original welded structure (Figure 3b). The connection of the top storage with the posts is secured through plate joining and fastened with screw connections (Figure 6c). All images in Figure 6 are details of the structural design created in PTC Creo.



(**a**) (**b**) (**c**)

Figure 6. Details of the connection of individual structural elements at selected locations of the assembled structure: (**a**) detail 1, (**b**) detail 2, (**c**) detail 3.

Two types of cross-sections, Bosch profile 80 × 80 mm and Bosch profile 80 × 40 mm, form the basis of the aluminum structure, as shown in Table 2. The remaining structural elements are the bottom anchor plates, connecting plates, and top mounting plates made of structural steel type S235JR.

Material sheets of the Al-Mg-Si alloy are freely available from Bosch Rexroth, and the material characteristics and mechanical properties of the AlMgSi alloy are outlined in Table 3.

The properties of the fastening material of the screws (used strength class 8.8), as well as the structural steel from which the connecting plates, top mounting plates, and anchoring plates are made, are described in Table 4.

The maximum allowable stress of individual structural elements made of aluminum alloy, in accordance with Equation (3), will be

$$\sigma_{D,AlMgSi\ 0.5\ F25} = \frac{R_e}{k} = \frac{200\ \text{MPa}}{2} = 100\ \text{MPa}. \tag{5}$$

3.3. Finite Element Model of Aluminum Profiles

There are three options when creating a finite element profile. The aluminum beam profile can be modeled using volume elements. With volume elements, it is necessary for the finite element mesh to consist of at least three to five elements across the thickness of the profile (2 mm). In such cases, the number of elements and the number of equations to be solved increase rapidly. From a time perspective, this approach is significantly demanding in terms of both time and computational resources.

Table 2. The shapes of the cross-sections of the Bosch Rexroth profiles used along with the basic dimensions and corresponding material.

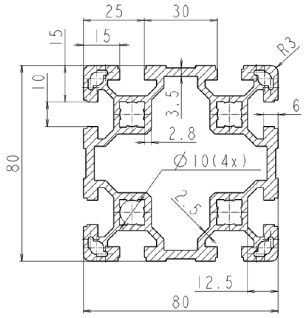
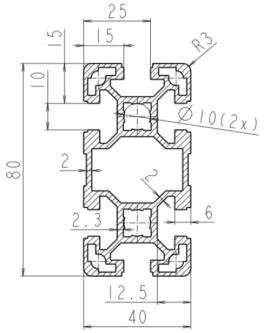
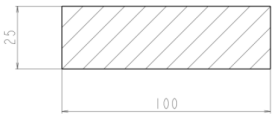
Used Profiles	Profile Cross-Section with Dimensions	Cross-Sectional Characteristics	Material
Bosch profile 80 × 80 L		A = 18.2 cm^2 I_x = 132.1 cm^4 I_y = 132.1 cm^4 W_x = 33.0 cm^3 W_y = 33.0 cm^3 m = 4.9 kg	ISO: AlMgSi 0.5 F25 U.S. equivalent: AW-6063-T66
Bosch profile 80 × 40 L mm		A = 9.9 cm^2 I_x = 63.4 cm^4 I_y = 17.3 cm^4 W_x = 15.9 cm^3 W_y = 8.7 cm^3 m = 4.9 kg	ISO: AlMgSi 0.5 F25 U.S. equivalent: AW-6063-T66
Connecting plate 25 × 100 mm		A = 25 cm^2 I_x = 63.4 cm^4 I_y = 17.3 cm^4	EN: S235JR (STN: 11 375)

Table 3. Material characteristics and mechanical properties of the AlMgSi alloy.

Material Type	Young's Modulus in Tension E [GPa]	Poisson's Ratio μ [-]	Yield Strength R_e [MPa]	Ultimate Strength R_m [MPa]
AlMgSi 0.5 F25	70	0.34	200	250

Using beam elements representing the prescribed profile is the least demanding in terms of geometry modifications. No geometry modifications are needed for the profile cross-section. This technique is frequently used in practice and provides a high degree of agreement with experimental measurements. However, in the case of the screw pretension, we are considering and assessing its impact on the individual parts of the structure, and this technique cannot be used.

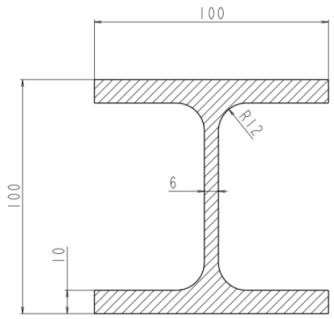
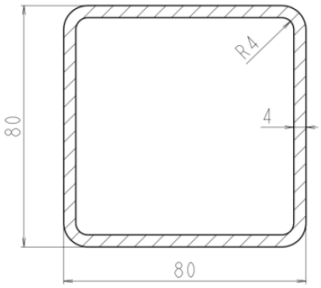
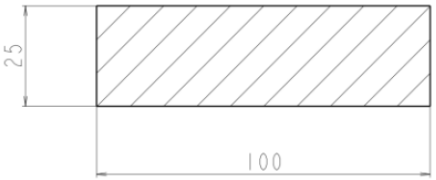
The most suitable modeling technique for our purposes is using shell elements. However, from the model preparation perspective, this is the most time-consuming approach due to the complexity of the cross-sections used. Therefore, Bosch profiles are modeled using shell elements. This approach is scarcely described by other authors.

The shell element creation technique requires geometry modifications, such as removing chamfers and the rounding of edges, so that center planes can be extracted from the volume model of the profile. These geometry modifications were made in the PTC Creo software, as shown in Figure 7.

The difference in the cross-sectional area of the Bosch profile with dimensions of 80 × 80 mm after modification is 0.5%. For the profile with dimensions of 80 × 40 mm, the difference in cross-sectional areas after modification is 10%, which is less significant

since these profiles are used as horizontal braces on the uprights and do not form the main load-bearing part of the structure.

Table 4. Dimensions of the cross-sections and materials of the individual parts of the structure.

Used Profiles	Cross-Section of the Profile with Dimensions	Material
I profile (HEB100)		EN: S235JR (STN: 11 375)
Jäkl profile (80 × 80 × 4)		EN: S235JR (STN: 11 375)
Top plate (25 × 100)		EN: S235JR (STN: 11 375)

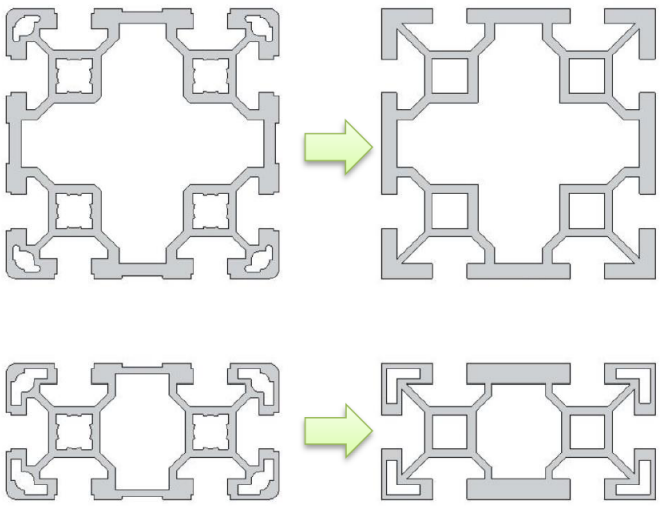
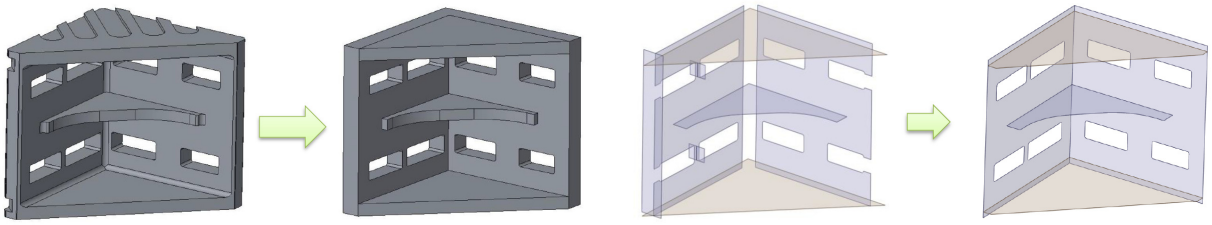


Figure 7. Original (on the **left**) and modified (on the **right**) cross-section geometry of the profiles used.

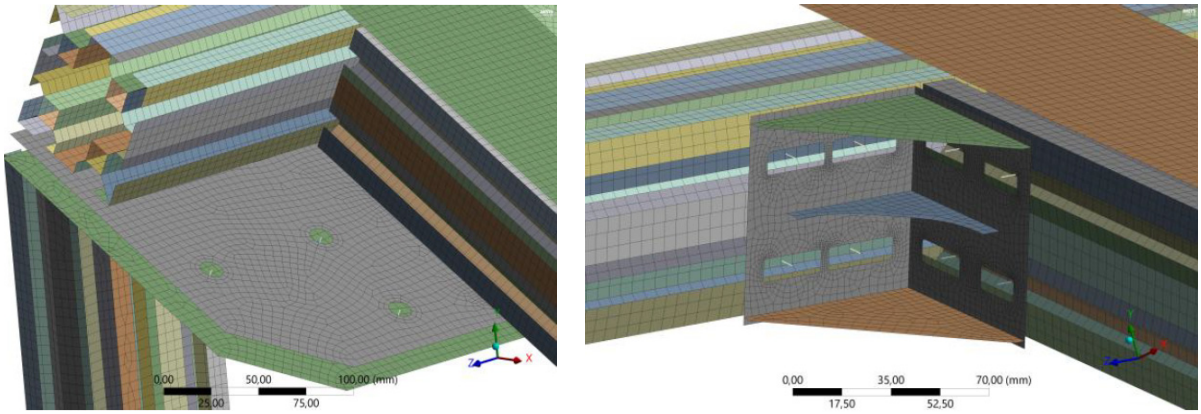
The process of modifying the geometry for the angle brackets to use shell elements is shown in Figure 8. The holes for the screws remain intact.

The element size is 5 mm, which is a sufficiently fine mesh for a structure with these dimensions. For the shell model, SHELL181 elements were used, and for the bolt connections, beam elements of type BEAM188 were used (see Figure 9).



(**a**) (**b**)

Figure 8. Modified geometry of the angle bracket: (**a**) removal of fillets and edges; (**b**) extracted mid-plane and compatible finite element model.



(**a**) (**b**)

Figure 9. Detail of the finite element mesh for shell and beam elements: (**a**) connection of the top seating plates with bolts; (**b**) connection of the angle bracket with the profile using bolts. All contact surfaces are connected by bolted joints.

The considered friction coefficient values are 0.15–0.2, depending on the type of material in contact, aluminum–steel or steel–steel. For shell elements, the shell thickness is set, which allows for contact detection at an offset distance.

3.4. Boundary Conditions and Loading of the Aluminum Profile Structure

The structure is loaded with its own weight. Axial force is applied to all screw joints in the structure based on the known value of the torque on the wrench used for tightening the screws. There are three groups of screw joints, and based on their size and type, we have the following axial preload values:

1. Hexagonal screws M14: connecting the storage to the uprights, M_k = 90 N·m. The resulting axial force is

$$F_{Q_1} = \frac{90,000}{\frac{12.701}{2} \cdot tg\left(arct\frac{2}{\pi\ 12.701} + arctg(0.12)\right) + 0.1\frac{22+15}{4}} \cong 44{,}700\ \text{N}. \quad (6)$$

2. Screws with a cylindrical head M8: connecting the top plates and the bottom seat plates to the storage frame, M_k = 8 N·m. The manufacturer specifies the maximum force F_{Q_2}max = 7000 N. The resulting axial force will be

$$F_{Q_2} = \frac{8000}{\frac{7.188}{2} \cdot tg\left(arct\frac{1.25}{\pi\ 7.188} + arctg(0.12)\right) + 0.1\frac{13+8.4}{4}} \cong 6850\ \text{N}. \quad (7)$$

3. Flanged screws M8: used in brackets, connecting the profiles, M_k = 8 N·m. Even though the same tightening torque is used as in the previous case, the screws have a larger seating area due to the different shape of the head, resulting in a lower axial force:

$$F_{Q_3} = \frac{8000}{\frac{7.188}{2} \cdot tg\left(arct\frac{1.25}{\pi\, 7.188} + arctg(0.12)\right) + 0.1\frac{20+18.7}{4}} \cong 5900 \text{ N}. \quad (8)$$

The weight of the upper fastening plates is F = 30,000 N in the direction of gravity. The defined boundary conditions are as follows: self-weight, fixation of the bottom of the uprights to the floor, loading of the storage, and preloading in the screws during their tightening in the assembly process (Figure 10).

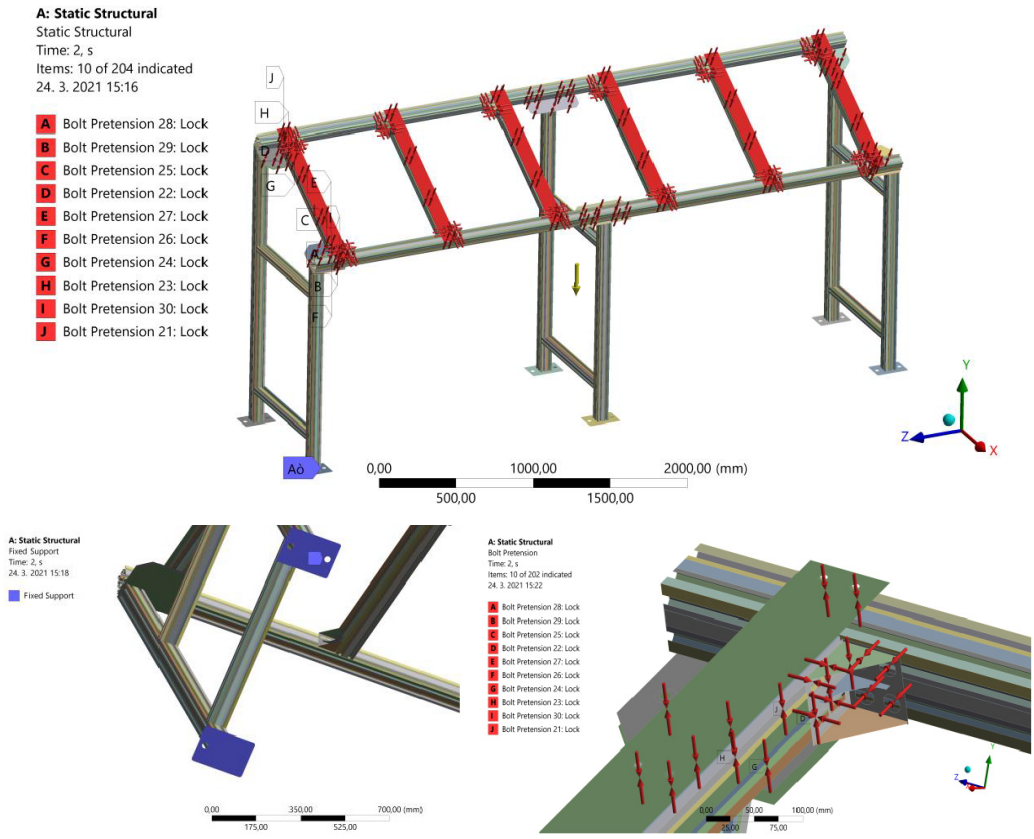


Figure 10. Details of the specified boundary conditions.

3.5. Results of the Structural Strength Analysis of the Aluminum Profile

The finite element analysis requires at least two time steps. In the first time step, the structure is loaded with its own weight, and the predefined preload in the screws, caused by their tightening, is applied (Figure 11). In the areas where the M14 screw washer makes contact, the stress values range between 40 and 50 MPa.

In the second time step, a continuous load representing the weight of all components stored on the shelf is applied. Three areas with the highest HMH stress values were identified throughout the structure. A detailed view of the first critical area is shown in Figure 12a.

Aside from the small local areas directly affected by the screw preload, the most stressed part of the first "critical area" is the transition between the Bosch profile column and the lower connecting plate. The HMH stress reaches a maximum value of nearly 31 MPa at the top of the profile, which corresponds to 31% of the design strength value.

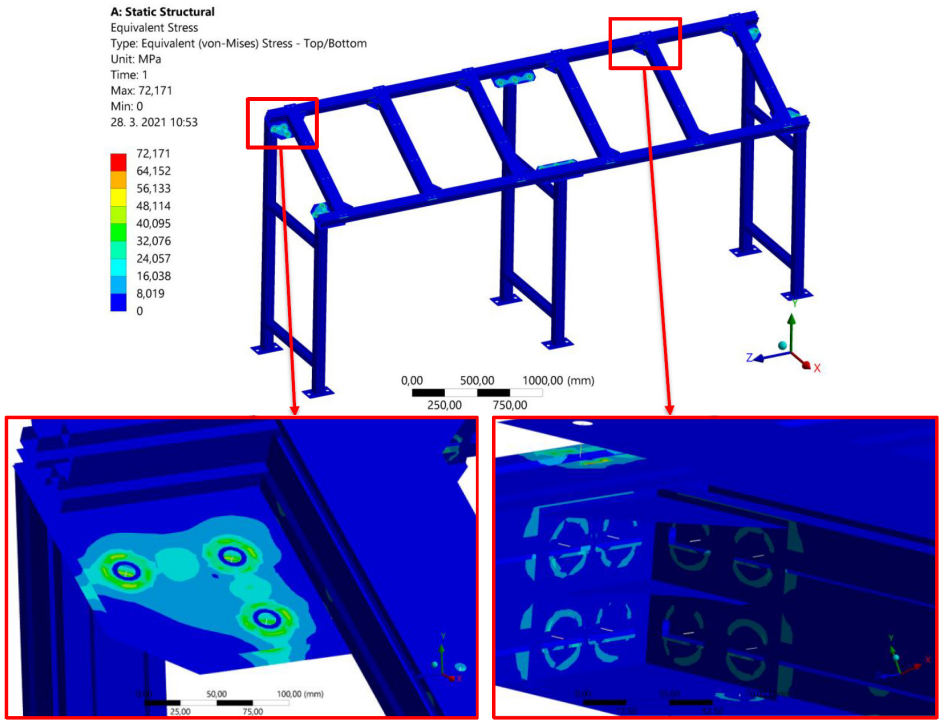
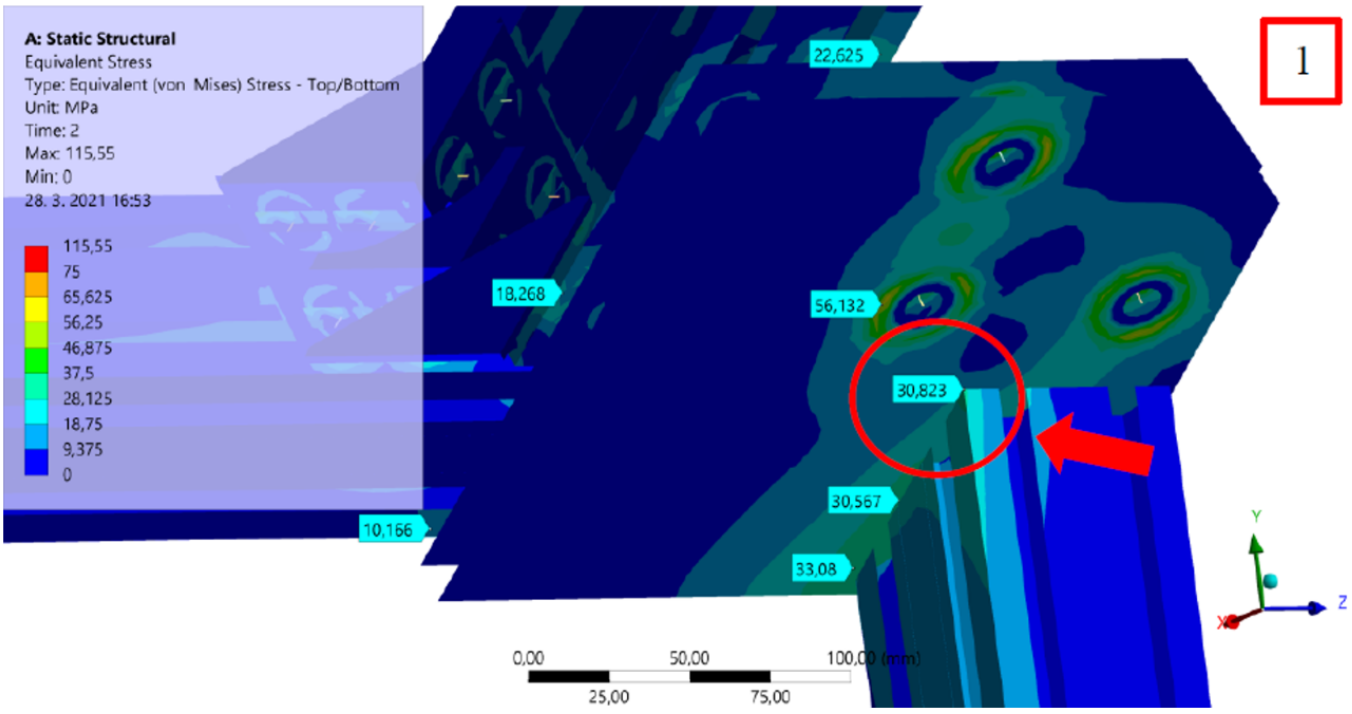


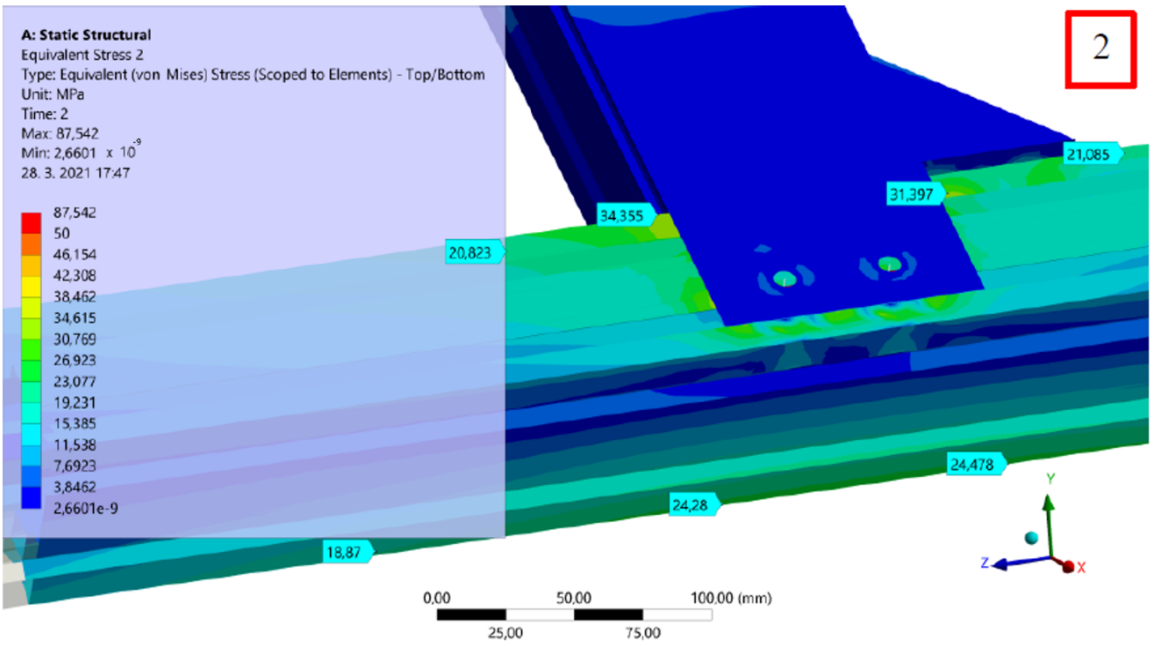
Figure 11. Detail of the HMH stress distribution in the rack structure, time step 1.

A closer view of the HMH stress distribution in the second most stressed area is shown in Figure 12b. In this region, bending stress has a significant effect, with the HMH stress in the Bosch profile reaching approximately 34 MPa (34% of the allowed stress value). Stress concentrators are in the areas where the Bosch profiles meet the reach values around 87 MPa. The HMH stress distribution in the third most exposed area is shown in Figure 13a.



(**a**)

Figure 12. *Cont.*

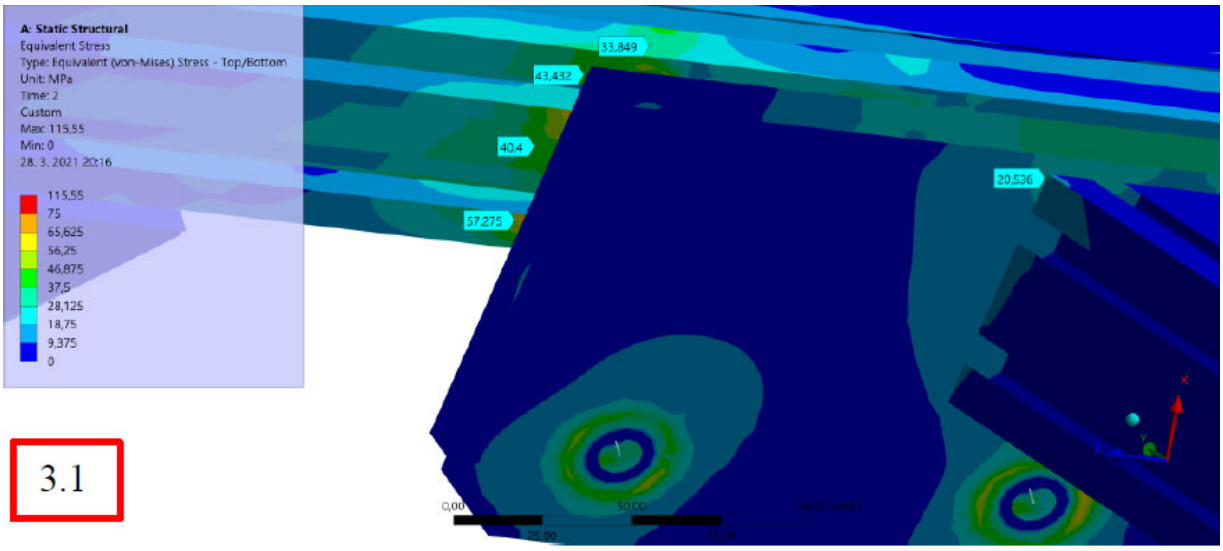


(**b**)

Figure 12. Detail of the HMH stress distribution: (**a**) first critical area; (**b**) second critical area.

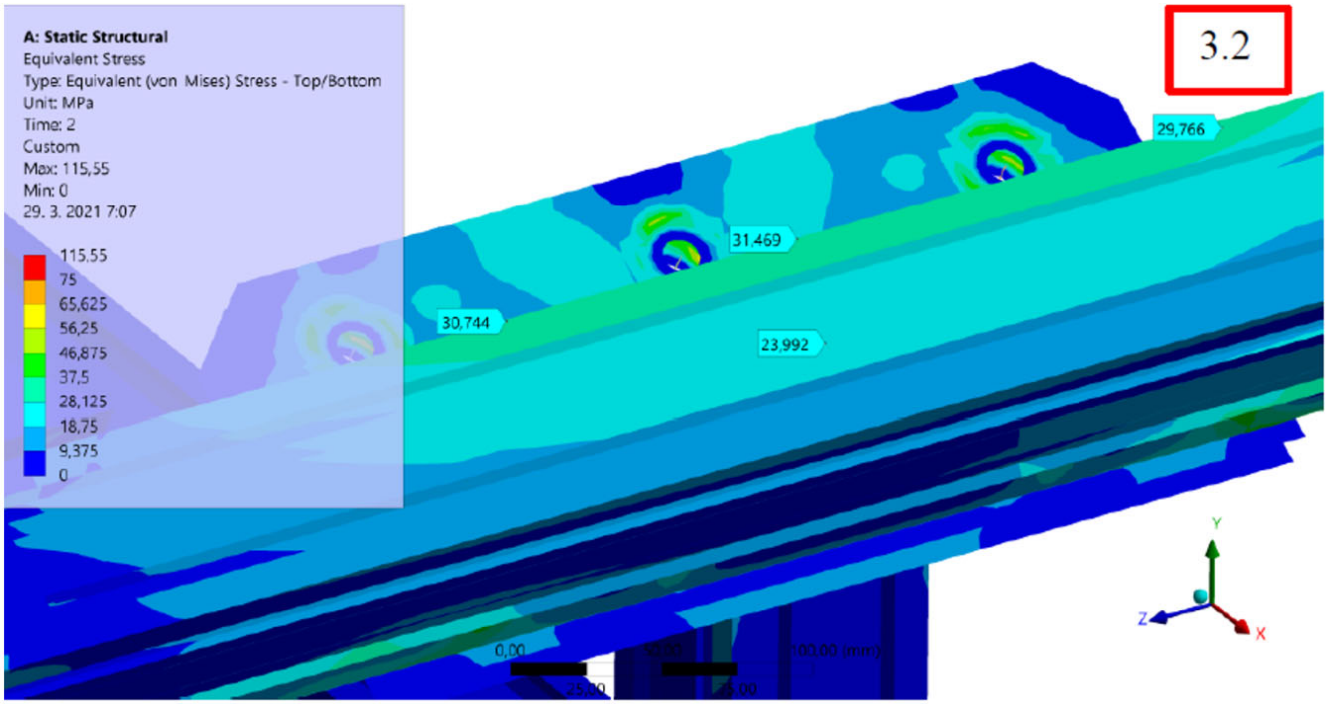
The most stressed location in this area is the transition region where the Bosch profile extends over the edge of the seating plate to which it is bolted. The highest HMH stress at this point reaches approximately 57 MPa, which corresponds to 57% of the material's required strength. An interesting observation is the distribution of HMH stresses in the upper part of the profile in this region, where stress in the most critical areas ranges from 20 to 32 MPa (Figure 13b).

The most stressed M14 screws are at the connection between the shelf and the columns, with stresses ranging from 190 to 495 MPa, where the highest values reach 78% of the yield strength. The maximum directional deformation along the Y-axis is 2.1953 mm.



(**a**)

Figure 13. *Cont.*



(**b**)

Figure 13. Detail of the HMH stress distribution in the third critical area: (**a**) bottom view; (**b**) top view.

3.6. Eigenvalue Buckling (Boss of Stability) of the Aluminum Profile

Due to the applied load, the aluminum structure may lose stability. Therefore, it is necessary to investigate the structure subjected to buckling. The first and most likely mode of stability loss is the buckling of the structure from its equilibrium position along the z-axis, shown in Figure 14. In this direction, the structure is not transversely reinforced.

The load multiplier reaches a value of 47.118, which means that an approximately 47 times greater load would need to be applied for the structure to lose stability and buckle out of equilibrium. The designed structure provides a sufficient safety margin.

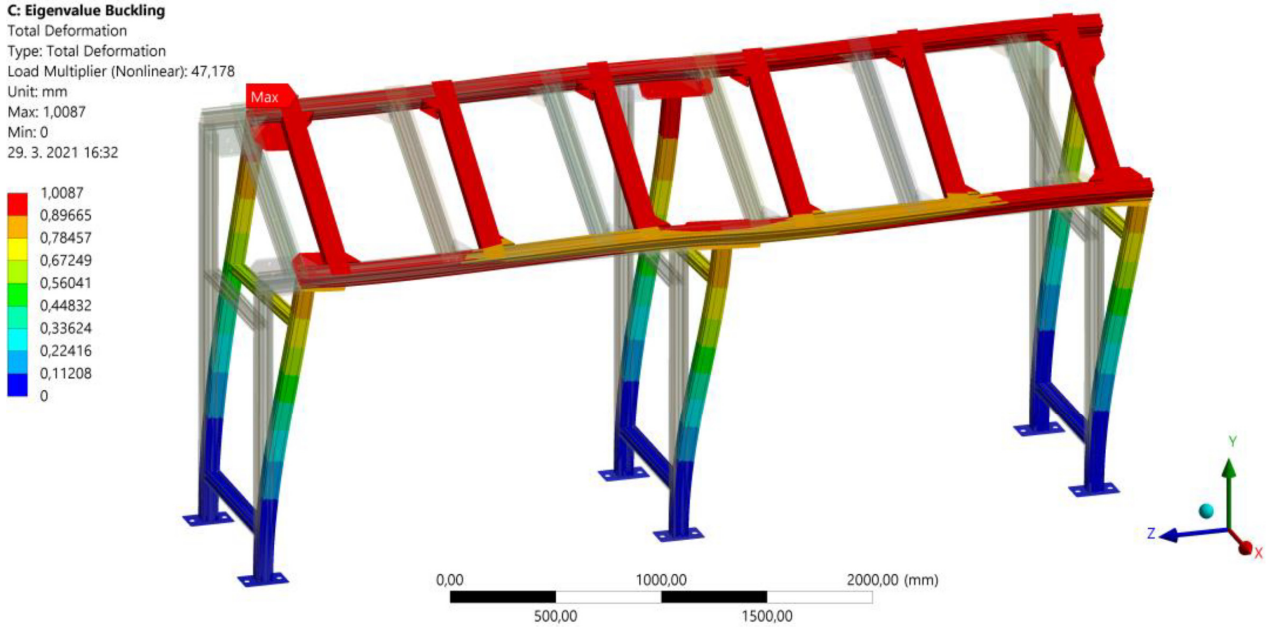


Figure 14. The first natural buckling mode of the aluminum structure.

4. Welded Rack Structure

4.1. Structural Model of the Welded Construction

For the finite element analysis, the model was created in the CAD software PTC Creo version 10.0.4.0 (Figure 3b). It consists of massive wide-flange I profiles of the H series. The horizontal crossbars on the posts are made from thin-walled (so-called Jäkl) profiles. The stiffness of the frame is also significantly influenced by the thick top plates placed at the upper part of the storage space, on which the welding fixtures will be mounted. The dimensions and cross-sections of the used profiles, as well as the corresponding materials, are listed in Table 4.

The mechanical properties of the materials used are described in Table 5. As can be seen from the previous Table 4, all structural elements of the welded subassemblies are made from the same type of construction steel, designated as S235JR. However, in Table 5, the mechanical properties of the connecting components are also defined according to ISO 898-1 [44], as the screw connections themselves will also be considered in the analysis.

Table 5. Mechanical properties of the materials used according to Standard EN 10025-2/04 [45] and ISO 898-1.

Material Type	Young's Modulus in Tension E [GPa]	Poisson's Ratio μ [–]	Yield Strength R_e [MPa]	Ultimate Strength R_m [MPa]
S235JR	200	0.3	240	360–510
Fastening material, strength class 8.8	200	0.3	640	800

In evaluating the ability of the shelving structure to reliably carry the given load, the relationship (1) will be used, with the minimum value of the safety factor based on practical requirements being considered as k = 2 for the load-bearing elements of the structure. For bolted joints, the safety factor will be considered as k = 1.3. Then, the maximum allowable stress in the individual structural parts will be

$$\sigma_{D,S235JR} = \frac{240\ \text{MPa}}{2} = 120\ \text{MPa}, \tag{9}$$

$$\sigma_{D,8.8} = \frac{640\ \text{MPa}}{1.3} \cong 492\ \text{MPa}. \tag{10}$$

To ensure the required strength in the welds, the allowable stress needs to be reduced by 30%, which is achieved by using the welding influence coefficient c:

$$\sigma_{D,Zv\ S235JR} = c \cdot \sigma_{D,S235JR} = 0.7 \times 120\ \text{MPa} = 84\ \text{MPa}. \tag{11}$$

4.2. Finite Element Shell Model of the Welded Structure

The created structural assembly requires a complete set of modifications to be suitably prepared for the finite element analysis. All I profiles need to be converted to shell elements since they are thin-walled profiles with a thickness of 4 mm, as shown in Figure 15. In finite element analyses using solid elements, the meshing of the profile wall would require three to four elements along the thickness of the profile. The element size used would also need to be maintained along the length of the profile to ensure correct element shapes without singularities. A defined thickness is then assigned to the shell element.

The use of shell elements for this structure, given its dimensions and the profiles used, still appears to be the most suitable option. Their main advantage in this context is the saving of computational time due to the significantly lower number of elements compared to the solid model. Easier mesh creation, faster postprocessing, and a lower

probability of negative Jacobian formation in thin structural elements also favor the use of shell elements [46]

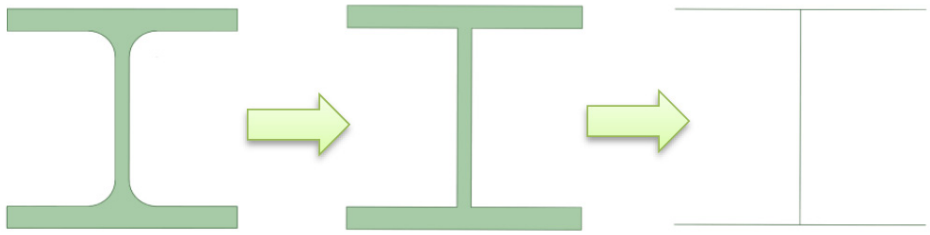


Figure 15. Preparation of the I profile for creating the shell model.

On the other hand, the disadvantage of this solution is the more demanding preparation of the model for extracting mid-plane definitions, as shown in Figure 16.

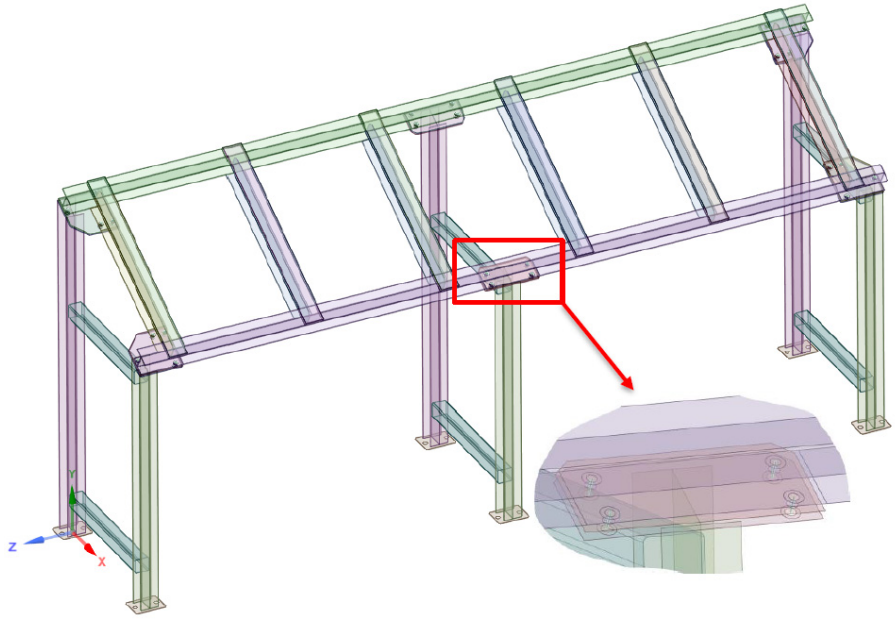


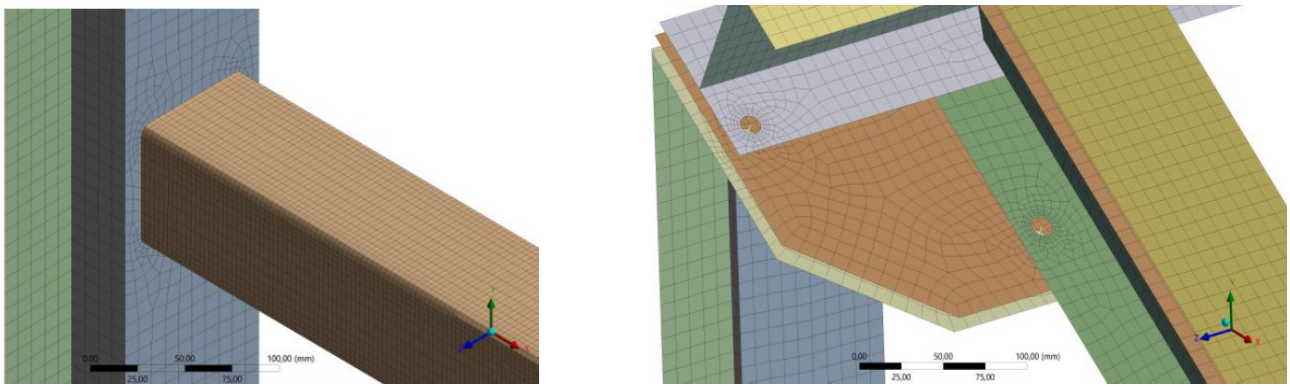
Figure 16. The shell model of the rack, including a zoomed-in detail of one of the connections.

The bolt connections joining the individual columns with the storage assembly will also be modeled using shell elements. The bolts themselves will be represented by beam elements, BEAM 188, with a minimum of two elements ensured. The advantage of using these over volume elements is, similar to the shell case mentioned earlier, a significant reduction in computational time, especially when there are several dozens of them in the model. This method is often used when analyzing the effects of prestress on the behavior of the entire structure under load. The main disadvantage of this modeling approach is that it is not possible to obtain results for the stress distribution along the bolt's cross-section.

The finite element quadrilateral mesh is created using the shell element type SHELL181. In areas with stress concentrators, the finite element mesh is refined (Figure 17a,b). The entire model consists of 173,217 elements with an element quality of 0.93.

4.3. Boundary Conditions and Loading of the Welded Structure

Based on the real conditions of the placement and loading of the rack structure in space, it is necessary to construct a suitable model of boundary conditions and loads that best approximate this actual state.



(**a**) (**b**)

Figure 17. Finite element mesh detail: (**a**) column with reinforcement; (**b**) base plates and I-profile.

The fixation of the model is defined by prescribing a single boundary condition—fixed support—on all surfaces of the anchor plates placed on the individual columns. The loading model is implemented as follows, in two steps:

- Considering the significant weight of the storage, the structure was loaded with its own weight using the "standard earth gravity" function. In the first step, bolt pretension was applied to all bolted joints in the structure using the "bolt pretension" function, which arises due to tightening the joints with a torque wrench. In this case, the known torque value M_k = 70 N·m applied during the tightening of the bolts is used, and the axial force in the bolt is calculated using the formula: [47]

$$M_K = F_Q \cdot \frac{d_2}{2} \cdot tg(\gamma + \phi') + F_Q \cdot f \cdot r_S. \tag{12}$$

The relationship for the axial force F_Q is as follows:

$$F_Q = \frac{M_K}{\frac{d_2}{2} \cdot tg(\gamma + \phi') + f \cdot r_S}, \tag{13}$$

where all the variables for the M12 bolt are summarized in Table 6.

Table 6. Variables in Equations (10) and (11).

Variable	Description	Variable Value
γ	Thread pitch angle	$\gamma = arctg\frac{p}{\pi \cdot d_2}$
p	Thread pitch value for the M12 screw	p = 1.75 mm
Φ'	Friction angle considering the thread profile	$tg\phi' = f' \cong 0.1 - 0.12$
f	Coefficient of friction between the nut (or screw head) and the material	$f \cong 0.1$
d_2	Mean thread diameter for the M12 screw	$d_2 = 10.863$ mm
r_S	Friction radius	$r_S = \frac{s+\delta}{4}$
δ	Hole diameter for the screw for M12	$\delta = 13$ mm
s	Hexagonal dimension of the nut or screw head for the M12 screw	$s = 19$ mm

After substituting all the values into Equation (13), we obtain the resulting axial force for the M12 hexagonal screw with a magnitude of

$$F_Q = \frac{70{,}000}{\frac{10.863}{2} \cdot tg\left(arctg\frac{1.75}{\pi\ 10.863} + arctg(0.12)\right) + 0.1 \cdot \frac{19+13}{4}} \cong 40{,}000\ \text{N}, \tag{14}$$

A contact is defined between the nut, the head of the screw, and the seating surfaces.

- In the next step, a continuous load of force with a magnitude of F = 30,000 N, acting in the direction of gravity, was applied to the surfaces of the upper plates. This force includes primarily the weight of the welding fixtures when the rack is fully loaded, along with the weight of other structural elements placed on the rack for securing the fixtures (cover plates, seating plates with encoding for recognizing the presence of a specific fixture type, etc.) (Figure 18).

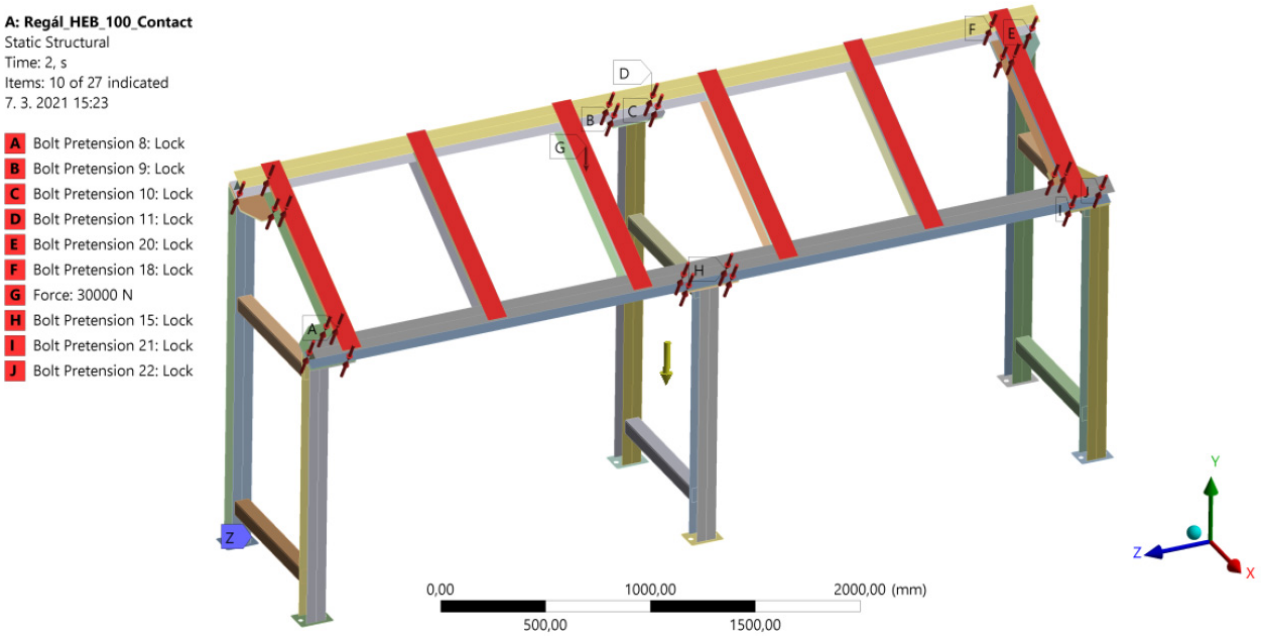


Figure 18. The shell model of the rack with beam-type bolted connections.

4.4. Results of the Strength Analysis of the Welded Structure

Disregarding small locations that are directly affected by the pretension from the bolted connections, the most stressed areas in the first region are those where the edge of one structural element connects or touches the surface of another structural element. In the upper part of the I-profile, at the point of contact with the connecting plate, the maximum HMH stress of 40.3 MPa occurs, which, considering the weld location, represents 47.98% of the allowable stress (Figure 19a).

In the second critical area, bending stress has a dominant effect, as this is the furthest point from the rack uprights, meaning this part is not supported from below. The maximum HMH stress here reaches 26.7 MPa, which represents 31.79% of the allowable stress, assuming it is a welded area (Figure 19b).

The largest deformations of the profiles occur in the direction of the applied weight of the welded fixtures, and the maximum values of directional deformation along the Y-axis reach 0.34 mm.

4.5. Eigenvalue Buckling (Loss of Stability) of the Welded Structure

For slender structures, it is necessary to perform a stability check in terms of safety and safe operation. The first natural buckling mode occurs in the transverse direction. The shelving structure is not reinforced in this direction and will deflect sideways along the z-axis, as shown in Figure 20. The load multiplier is 167.27, meaning that in order for the structure to lose its equilibrium, the applied load must be 167.27 times greater than the defined load.

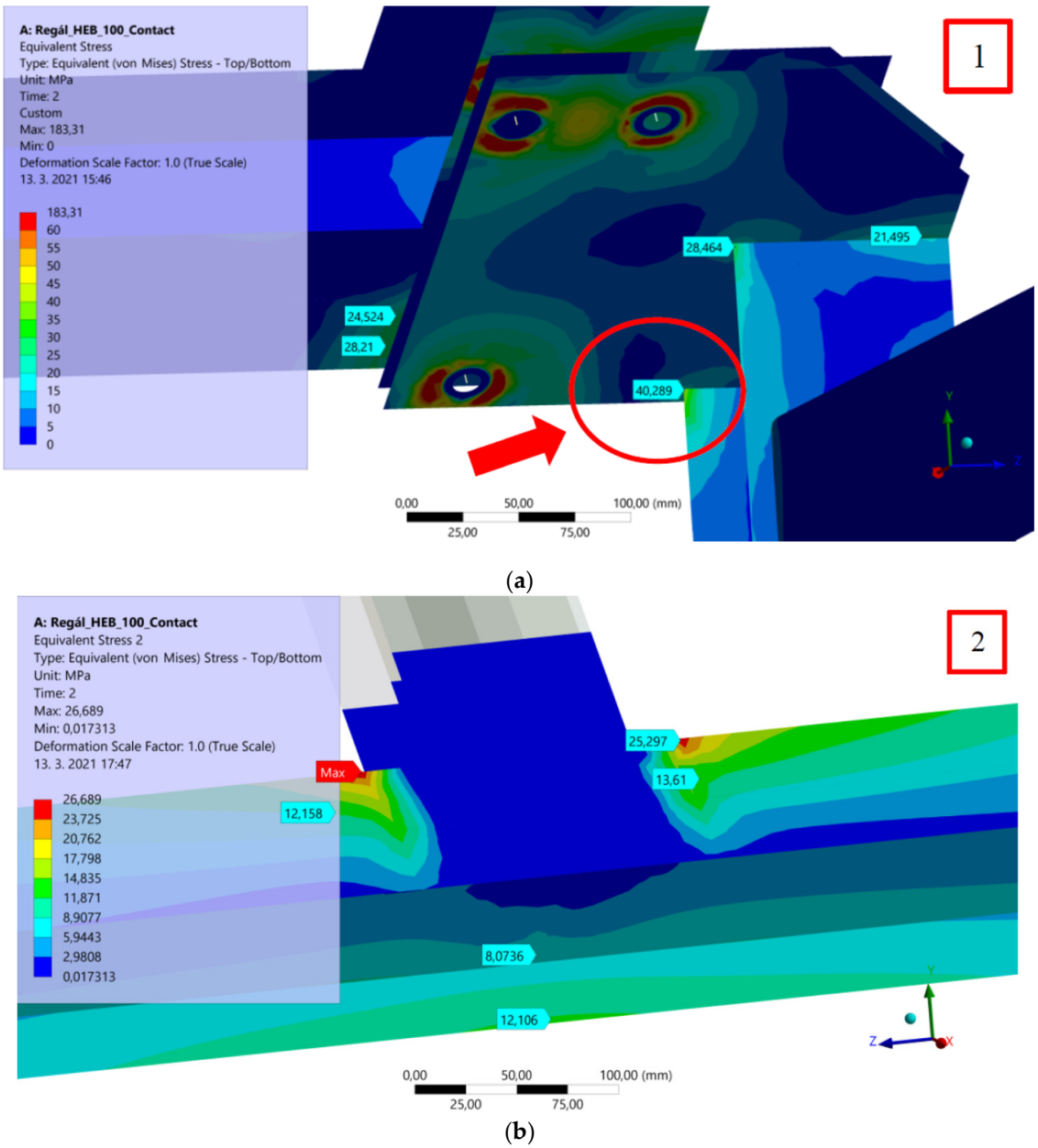


Figure 19. Detail of the distribution of HMH stress in the welded structure: (**a**) first critical area—in circle; (**b**) second critical area.

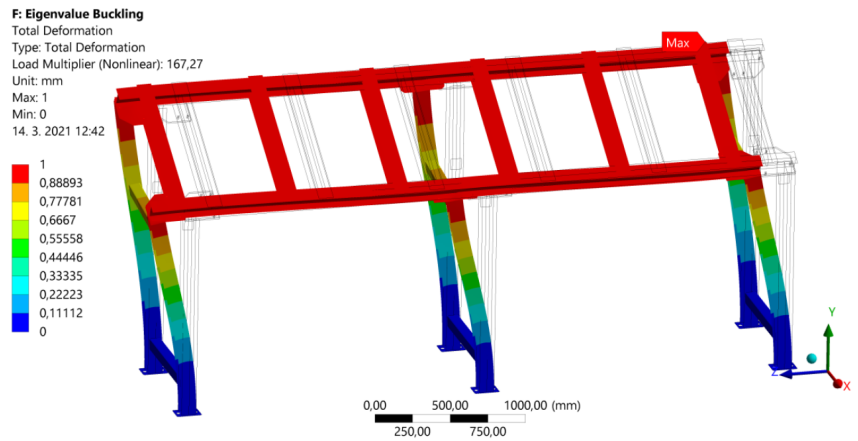


Figure 20. First natural buckling mode of the welded structure.

5. Cost Comparison from an Economic Perspective

The main comparison criterion is the total cost of both solutions. This includes, of course, the cost of raw materials as well as the production and labor costs. The financial information in Figure 21 is directly obtained from a company that manufactures commercial rack structures. All the main factors that contribute to the price in both solutions are as follows:

(a) Assembled variant

- Input materials (Bosch profiles, plates, and fastening materials—bolts, angle brackets, T-nuts);
- Cutting profiles to the required dimensions;
- Welding of the structure;
- Milling parts of the structure—drilling cylindrical recesses into plates for bolts with a cylindrical head;
- Assembly of the structure.

(b) Welded variant

- Input materials (I profiles, Jäkl profiles, plates, and fastening materials—bolts);
- Cutting of semi-finished products to the required dimensions;
- Welding of the structure;
- Milling parts of the structure—the storage (adjusting the top plates and drilling mounting holes);
- Spraying the structure;
- Assembly of the structure.

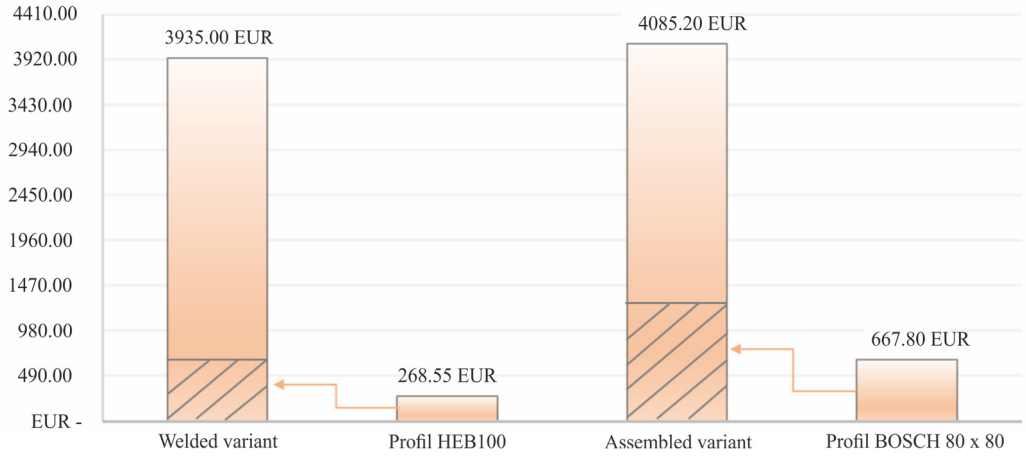


Figure 21. Price comparison of the proposed variants.

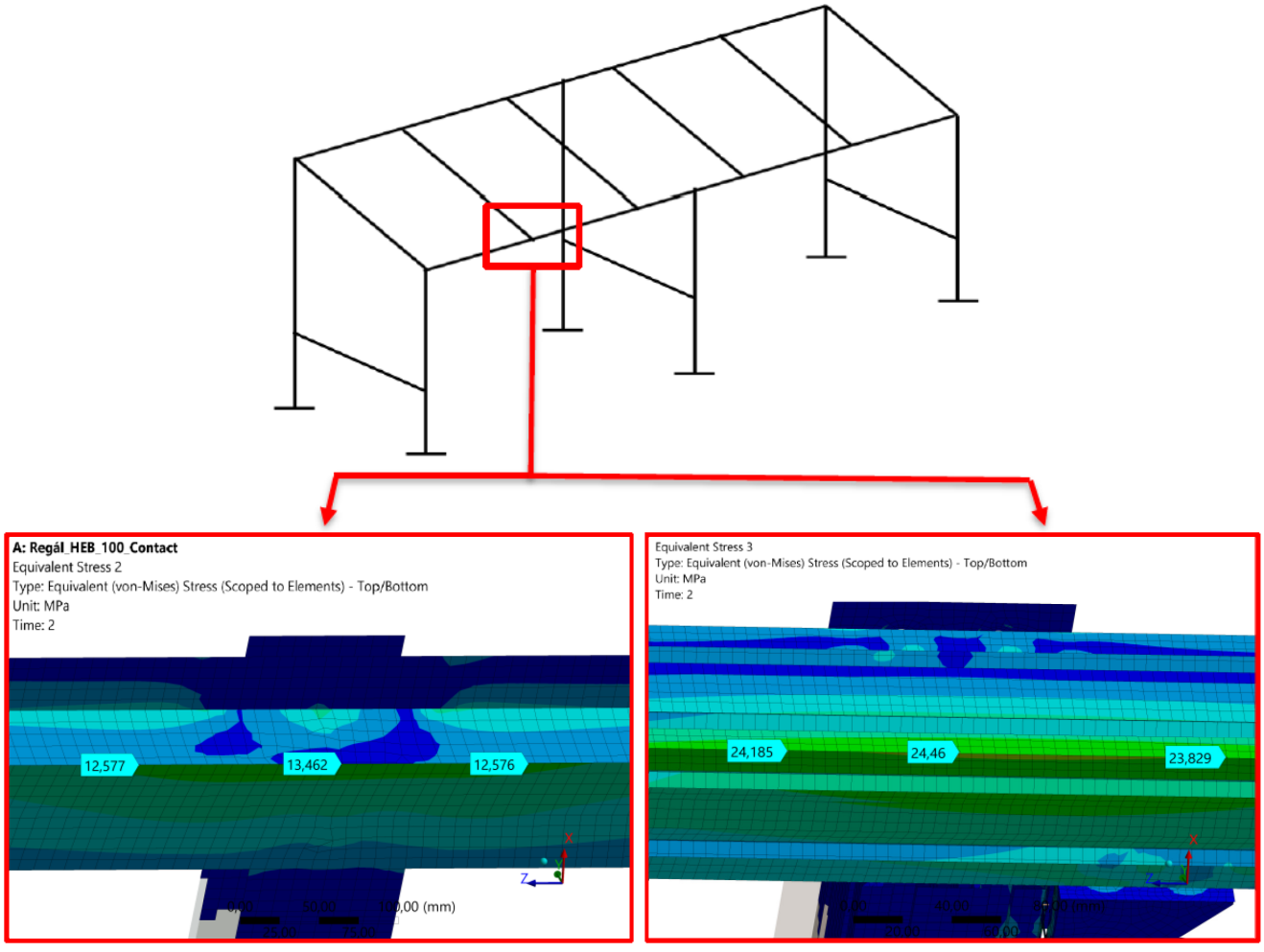
The purchase price of the Bosch profile 80 × 80 is approximately 2.5 times higher compared to the rolled HEB100 profile. However, this significant price difference in the profiles, which form the basis of both constructions, surprisingly did not result in a major cost difference between the two variants. Therefore, it can be concluded that the higher purchase price of the Bosch profiles in the context of the entire rack is compensated by savings in costs associated with welding and surface treatment operations.

However, the price of the assembled aluminum construction is still approximately 4% higher compared to the welded steel construction, as shown in Figure 21. Considering the countless advantages that the use of Bosch profiles offers in the field of the automated industry, this difference is relatively negligible. Constructions made from these profiles can be repeatedly, flexibly, and fairly easily reconfigured, as dismountable types of connections are used. The simple handling during assembly is related to the relatively low weight of the

profiles. Tasks associated with the requirement for additional protective coverings or any component to be added to an already existing structure are saved from time-consuming manual threading in the required locations. This function is replaced by the profile groove in aluminum Bosch profiles, along with the use of Bosch stones. These mentioned benefits are difficult to quantify financially.

6. Comprehensive Comparison of Variants and Discussion of the Obtained Results

It is important to note that the verification of the constructions' ability to safely carry the required load was the starting assumption and a fundamental condition for such a comparison. If this fundamental criterion had not been met, the price comparison of variants would not have been justified. The performed strength analyses of the load-bearing parts of the constructions, however, showed satisfactory results in both cases, and no structural modifications were necessary for either variant. Despite this, it is useful to compare the stress distribution of the selected location for both the welded and assembled constructions in order to gain a better understanding of the differences in theoretical strength reserves between these solutions, as shown in Figure 22.



(**a**) (**b**)

Figure 22. Comparison of the distribution of Equivalent von-Mises stresses in the selected location: (**a**) the welded constructions; (**b**) assembled aluminum constructions.

The data from Figure 22 are used in Table 7, which also includes the calculated safety factors for both variants at the given location of the structure. The maximum value of

equivalent stress in the welded structure is σ = 13.5 MPa (Figure 22a), and in the assembled structure it is σ = 24.5 MPa (Figure 22b). Taking into account the yield strength of the respective materials, the safety factor is determined using Equation (13).

$$k = \frac{R_e}{\sigma}. \tag{15}$$

where R_e is the yield strength [MPa] and σ is the maximum value of equivalent stress at the given location [MPa].

Table 7. Comparison of the solutions.

Construction Variant	Maximum Value of Equivalent Stress at the Given Location [MPa]	Yield Strength [MPa]	Safety Factor [-]
Welded	13.5	240	17.8
Assembled	24.5	200	8.2

From Table 7, it is evident that the welded variant has twice the safety margin compared to the assembled variant at this location of the structure, which is understandable given the predominant bending stress in this area and the robustness of the steel profiles used. However, both solutions are over-dimensioned with sufficient strength reserves, and this comparison serves merely as a brief final summary of the strength calculations for these construction variants.

7. Conclusions

The purpose of this article was to compare and comprehensively analyze two structural design approaches for an industrial rack: the conventional welded structure made of Jäkl profiles and an alternative newly proposed assembled structure using aluminum Bosch Rexroth profiles. The results are applied to a specific profile type that is commonly utilized in practical engineering applications.

To achieve this objective, finite element analysis (FEA) methodologies were proposed and described, followed by a detailed FEM analysis of both solutions in terms of strength, stability loss, and Eigenvalue Buckling. The main contribution of this article lies in the application and validation of an advanced modeling approach using shell elements for aluminum profiles, which required geometric modifications and the extraction of mid-surfaces. A new and comprehensive approach was applied to address the given issue. The advantage of this approach—comparing two methods and conducting an economic analysis—was the ability to perform the most thorough possible assessment. Based on the conclusions of an extensive literature review, it can be stated that no similar comprehensive approach has been identified in any other research. The chosen shell element modeling approach delivers reliable results while reducing computational time and hardware demands.

Another significant component is the consideration of bolt preloading and its effect on the overall stress state in the structure, which provides a more realistic idea of the behavior of assembled systems in operation. The impact of bolt preloading on the overall stress state in the structure was also taken into account. The analysis results were compared.

The authors also conducted an economic analysis of both compared solutions. The results and their thorough analysis indicate that the modular structure made of aluminum profiles also offers significant variability and easy reconfiguration, which aligns with the requirements of modern industrial automation and the concept of “soft automation.” At the same time, the analysis confirmed the sufficient strength and stability of the selected aluminum profiles, while the welded steel structure offers a higher safety margin.

Based on the economic analysis, it can be stated that despite the higher acquisition cost of aluminum profiles, the overall costs of both solutions are comparable, with the aluminum profile solution being approximately 4% more expensive. The analysis took into account the costs of material procurement, processing, labor, and the technology required for assembly. The main contribution of the conducted analyses is the confirmation of the suitability of using the alternative solution based on aluminum profiles. Advantages such as flexibility, easy reconfiguration, and lower weight are difficult to quantify, but from the perspective of maintenance and adaptability, they represent a clear benefit.

The final selection of a specific variant, however, ultimately depends on the designer's decision based on the given circumstances, as in certain conditions, a structure with a higher safety factor may be more appropriate. The results of this comparison can serve as a methodological basis for making informed decisions regarding the appropriate structural solution for frame constructions in industrial applications.

Author Contributions: Conceptualization, L.J. and F.S.; methodology, L.J.; software, M.V.; validation, L.J., M.V. and F.S.; formal analysis, L.J.; investigation, F.S.; resources, L.J.; data curation, M.V.; writing—original draft preparation, F.S.; writing—review and editing, M.V.; visualization, L.J.; supervision, F.S.; project administration, L.J.; funding acquisition, M.V. All authors have read and agreed to the published version of the manuscript.

Funding: This research work was supported by the grant project KEGA 002ŽU-4/2023, 005ŽU-4/2024 and VEGA 1/0753/24.

Data Availability Statement: All data is provided in this article.

Conflicts of Interest: The authors declare no conflict of interest.

References

1. Huang, J.; Arinez, J. Modeling and Dynamic Assignment of the Adaptive Buffer Spaces in Serial Production Lines. *J. Manuf. Sci. Eng.* **2021**, *143*, 031005. [CrossRef]
2. Benito, R.; Hurtado, S.; Miguel, P.; Carazas, G. Optimization of the Stacking Process of Wire Mesh Coils in Industrial Processors. In Proceedings of the 5th International Conference of the Industrial Engineering and Industrial Management (IEIM), Nice, France, 10–12 January 2024; Volume 2070, pp. 100–111. [CrossRef]
3. Loske, D.; Koreis, J.; Klumpp, M. Golden Zone Storage Assignment and Picking Performance: An Empirical Analysis of Manual Picker-to-Parts OP Systems in Grocery Retailing. *IFAC-PapersOnLine* **2022**, *55*, 508–513. [CrossRef]
4. Molina, E.; Horvath, L.; West, R. Development of a Friction-Driven Finite Element Model to Simulate the Load Bridging Effect of Unit Loads Stored in Warehouse Racks. *Appl. Sci.* **2021**, *11*, 3029. [CrossRef]
5. Ozkal, F. Effects of Steel Bolts on Retrofitting the Buckling Performance of Storage Rack System Uprights. *Structures* **2024**, *64*, 106578. [CrossRef]
6. Ungermann, D.; Lemanski, T.; Brune, B.; Weiss, N.; Schulz, A.; Gosling, P. Optimized Shelving Racks through the Use of High-Strength Steel. *Stahlbau* **2023**, *92*, 495–507. [CrossRef]
7. Heo, G.; Choi, G.; Baek, E.; Kim, C. Development of Viscoelastic Damper System to Improve Seismic Performance of Storage Racks. *KSCE J. Civ. Eng.* **2021**, *25*, 3390–3400. [CrossRef]
8. Hu, D. Automated Pallet Racking Examination in Edge Platform Based on MobileNetV2: Towards Smart Manufacturing. *J. Grid Comput.* **2024**, *22*, 20. [CrossRef]
9. Blatnicky, M.; Dizo, J.; Barta, D.; Drozdziel, P. Engineering Design and Strength Analyses of Main Load-Bearing Parts of a Mechanical Rack System. *Diagnostyka* **2018**, *19*, 97–104. [CrossRef]
10. Liu, S.; Pekoz, T.; Gao, W.; Zieman, R.; Crews, J. Frame Analysis and Design of Industrial Rack Structures with Perforated Cold-Formed Steel Columns. *Thin-Walled Struct.* **2021**, *163*, 107755. [CrossRef]
11. Peng, D.; Wang, Z.; Sha, C. Analysis of the Effects of Back-stayed Arrangement on the Mechanical Properties of Corbel Shelf. In Proceedings of the International Conference on Mechanical, Manufacturing, Modeling and Mechatronics (IC4M), Kuala Lumpur, Malaysia, 27–29 February 2016. [CrossRef]
12. Marinopoulou, E.; Tsavdaridis, K.D.; Efthymiou, E. Modern Design Methods on Optimised Novel Aluminium Profiles. *Buildings* **2022**, *12*, 1904. [CrossRef]

13. Lutomirska, M.; Lutomirski, T. A Practical Case Study on Assessment and Rehabilitation of a Pipe Rack. *Eng. Fail. Anal.* **2022**, *141*, 106654. [CrossRef]
14. Faria, V.; Freitas, M.; Brandao, A. Reliability of Rack Columns Designed by the Direct Strength Method. *Struct. Eng. Int.* **2024**, *34*, 211–218. [CrossRef]
15. Alvarez, O.; Maureira, N.; Nunez, E.; Sanhueza, F.; Videla, A. Numerical Study on Seismic Response of Steel Storage Racks with Roller Type Isolator. *Metals* **2021**, *11*, 158. [CrossRef]
16. Mohamed, M.; Khalifa, W.; Mahmoud, M. Failure Analysis of Alloy Boron Steel Bolts in Steel Structure Assembly. *J. Fail. Anal. Prev.* **2022**, *23*, 88–98. [CrossRef]
17. Ziambaev, N. Analysis of Oscillations of Framework at Pulse Influence Taking into Account Physical Non-Linearity. In Proceedings of the International Conference on Construction, Architecture and Technosphere Safety (ICCATS), Chelyabinsk, Russia, 26–28 September 2018. [CrossRef]
18. Muniandy, V. Development of Racking and Irrigation System for Industrial Revolution 4.0 Vertical Farming. In Proceedings of the IEEE Conference on Technologies for Sustainability (SusTech), Virtual, 21–23 April 2022; pp. 132–135. [CrossRef]
19. Zhang, W.; Yu, C.; Tong, G. Model Analysis of Steel Frame Structures Considering Interactions between Racks and the Frame. *Buildings* **2023**, *13*, 1732. [CrossRef]
20. Ochrymiuk, T.; Dudda, W.; Froissart, M.; Badur, J. Principles of Stress-Strength Modelling of the Highly Thermally Loaded Materials-The Influence of an Effect of Strength Differential on the Material Effort. *Materials* **2022**, *14*, 7449. [CrossRef]
21. Taranu, G.; Iacob, S.; Taranu, N. Buckling Behavior of Perforated Cold-Formed Steel Uprights: Experimental Evaluation and Comparative Assessment Using FEM, EWM, and DSM. *Buildings* **2025**, *15*, 1561. [CrossRef]
22. Noonan, A.J.C.; Cameron, P.M.N.; Dofher, K.; Sukkasam, N.; Liu, T.; Rönn, L.; Monshupanee, T.; Hallam, S.J. An Automated High-Throughput Lighting System for Screening Photosynthetic Microorganisms in Plate-Based Formats. *Commun. Biol.* **2025**, *8*, 438. [CrossRef]
23. Yu, Y.; Li, Y.; Xie, F.; Song, J.; Bai, Y.; Fan, Y. Design and Experiment of Key Components of an Insertion Vegetable Grafting Machine with Six Plants Synchronous. *Sci. Rep.* **2025**, *15*, 16650. [CrossRef]
24. Shaker, F.M.F.; Mamdooh, Z.; Deifalla, A.; Yehia, M.M. Experimental Investigations of the Behavior of Stiffened Perforated Cold-Formed Steel Sections Subjected to Axial Compression. *Buildings* **2022**, *12*, 812. [CrossRef]
25. Baek, S.; Won, J.; Jang, S. Economic Integrated Structural Framing for BIM-Based Prefabricated Mechanical, Electrical, and Plumbing Racks. *Appl. Sci.* **2023**, *13*, 3677. [CrossRef]
26. Vujanac, R.; Živković, M.; Slavković, R.; Vulović, S. Steel Frame versus Rack Supported Warehouse Structures. *Teh. Vjesn.—Tech. Gaz.* **2017**, *24*, 1269–1276. [CrossRef]
27. Mela, K.; Heinisuo, M. Weight and Cost Optimization of Welded High Strength Steel Beams. *Eng. Struct.* **2014**, *79*, 354–364. [CrossRef]
28. Bernuzzi, C.; Pellegrino, C.; Simoncelli, M. Characterization of Existing Steel Racks via Dynamic Identification. *Buildings* **2021**, *11*, 603. [CrossRef]
29. Deng, Z.; Shang, Y. Size-Dependent Finite Element Analysis of Functionally Graded Flexoelectric Shell Structures Based on Consistent Couple Stress Theory. *Aerospace* **2024**, *11*, 661. [CrossRef]
30. Panchenko, S.; Gerlici, J.; Vatulia, G.; Lovska, A.; Pavliuchenkov, M.; Kravchenko, K. The Analysis of the Loading and the Strength of the FLAT RACK Removable Module with Viscoelastic Bonds in the Fittings. *Appl. Sci.* **2022**, *13*, 79. [CrossRef]
31. Choi, H.; Yoon, H.; Jung, E.; Lee, D. Structural Stability Assessment for Optimal Order Picking in Box-Stacked Storage Logistics. *Sensors* **2025**, *25*, 1085. [CrossRef]
32. He, M.; Guan, Z.; Hou, G.; Wang, X. A Novel Parts-to-Picker System with Buffer Racks and Access Racks in Flexible Warehousing Systems. *Sustainability* **2024**, *16*, 1388. [CrossRef]
33. Saderova, J.; Rosova, A.; Sofranko, M.; Kacmary, P. Example of Warehouse System Design Based on the Principle of Logistics. *Sustainability* **2021**, *13*, 4492. [CrossRef]
34. Houska, P.; Caisova, K.; Sitar, V.; Michna, S.; Alfonso, T. The Effect of Laser Welding Parameters on Aluminium PV Construction Rack Systems. *Manuf. Technol.* **2024**, *24*, 47–52. [CrossRef]
35. Bove, O.; Casafont, M.; Bonada, J.; Ferrer, M.; Lopez, F. Investigation on the Down-Aisle Ductility of Multiple Bay Pallet Racks by Means of Pushover Analyses. *Eng. Struct.* **2023**, *286*, 116085. [CrossRef]
36. Kouloughli, S.; Feciane, M. Mobile Rack AS/RS Dimensions Optimization for Single Cycle Time Minimization. *Int. J. Adv. Manuf. Technol.* **2022**, *121*, 1815–1836. [CrossRef]
37. Molina, E.; Horvath, L. Development of a Gaussian Process Model as a Surrogate to Study Load Bridging Performance in Racked Pallets. *Appl. Sci.* **2021**, *11*, 11865. [CrossRef]
38. Zhai, M. Optimizing Rack Locations in the Mobile-Rack Picking System: A Method of Integrating Rack Heat and Relevance. *Mathematics* **2024**, *12*, 413. [CrossRef]

39. Dudda, W.; Kraszewski, B. A Theoretical Validation of Burzynski Hypothesis for a Stress-Strain Analysis of Heat-Resistant Steel. *Case Stud. Therm. Eng.* **2021**, *23*, 100806. [CrossRef]
40. Lutz, A.; Halseid, M.; Graeve, I. Corrosion Performance of Powder-Coated Aluminum Profiles with Increased Trace Element Content. *Mater. Corros.* **2022**, *73*, 1575–1585. [CrossRef]
41. Fan, L.; Wang, F.; Wag, Z. Study on the Influence of Surface Treatment Process on the Corrosion Resistance of Aluminum Alloy Profile Coating. *Materials* **2023**, *16*, 6027. [CrossRef]
42. Güler, S.; Karagülle, H. Finite Element Analysis of Structures with Extruded Aluminum Profiles Having Complex Cross Sections. *Lat. Am. J. Solids Struct.* **2016**, *13*, 1499–1514. [CrossRef]
43. Jiang, Z.; You, B.; Huang, Z.; Zhang, G.; Hu, Q. Cross-Rack Update Bandwidth for Distributed Storage Systems. In Proceedings of the IEEE Global Communications Conference (GLOBECOM), Kuala Lumpur, Malaysia, 4–8 December 2023; pp. 3699–3704. [CrossRef]
44. *ISO 898-1*; Mechanical Properties of Fasteners Made of Carbon Steel and Alloy Steel. International Organization for Standardization: Geneva, Switzerland, 2013.
45. *EN 10025-2:2004*; Hot rolled products of structural steels. Part 2—Technical delivery conditions for non-alloy structural steels. CEN (European Committee for Standardization): Brussels, Belgium, 2004.
46. Broekaart, D. 5 Reasons Why Your FEA Simulations Should Be Set Up Using a Mid-Surface Shell Mesh for Thin-Walled Parts. Available online: https://blog.technia.com/en/simulation/why-setup-fea-with-a-mid-surface-shell-mesh-for-thin-walled-parts (accessed on 20 March 2025).
47. Bocko, P.; Mantič, M.; Kuľka, J. Input Parameters for the Calculation of Prestressed Bolted Joints in FEM. 2006. Available online: http://pbocko.szm.com/projects/publications/2006/vstupne%20parametre%20pre%20vypocet%20PSS%20v%20MKP%20BMK.pdf (accessed on 20 March 2025).

Disclaimer/Publisher's Note: The statements, opinions and data contained in all publications are solely those of the individual author(s) and contributor(s) and not of MDPI and/or the editor(s). MDPI and/or the editor(s) disclaim responsibility for any injury to people or property resulting from any ideas, methods, instructions or products referred to in the content.